Chapter 7.

Fluid mixing.

September_20_2016.

1. Introduction.

Fluid mixing plays a major role in many discussions of the formation of mineralising systems. The bringing together of two or more fluids with different redox states in order to deposit gold is appealing because it seemingly enables a fluid with gold in solution to be brought into a part of the mineral phase diagram where gold has low equilibrium solubility. The fluid mixing here occurs across the interface between two fluids so that gold deposition is restricted to positions on that interface.

Models for fluid mixing geometry in mineral systems are numerous but essentially are of the form illustrated in Figure 7.1 (a). Here meteoric or basinal fluids are drawn down by a mechanism that is rarely specified. Topographically driven flow is one of the few ways of achieving such downward flow although the mechanism of driving basinal fluids downwards into a region of lithostatically pressured fluids is not clear. In general models such as depicted in Figure 7.1 (a) are hydrologically inadmissible since they postulate downward flow (necessitating a sub-hydrostatic fluid pressure gradient) with continuous hydrological connection into upward flow regions (necessitation a super-hydrostatic fluid pressure gradient).

The fluid mixing concepts are called upon to explain observations such as shown in Figure 7.1 (b and c). Here localised mineral assemblages stable under oxidised conditions (magnetite-bearing) are embedded in a “sea” of mineral assemblages stable under reduced conditions (pyrrhotite/pyrite-bearing). High gold deposits are concentrated near the boundaries between these two regions (Figure 7.1 c).

The details of processes and problems involved in mixing across an interface between two fluids of different redox staes are discussed in Section 7.2. For the moment we present an alternative interpretation of Figures 7.1 (b, c) that does not involve the mixing of two or more fluids.

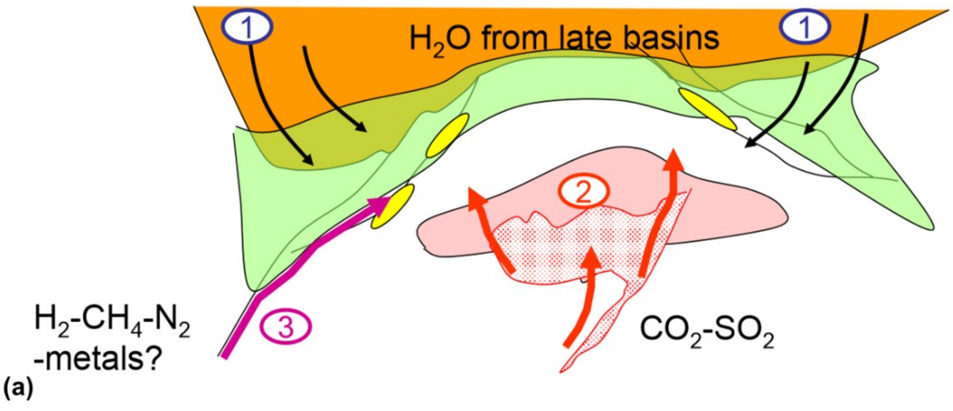

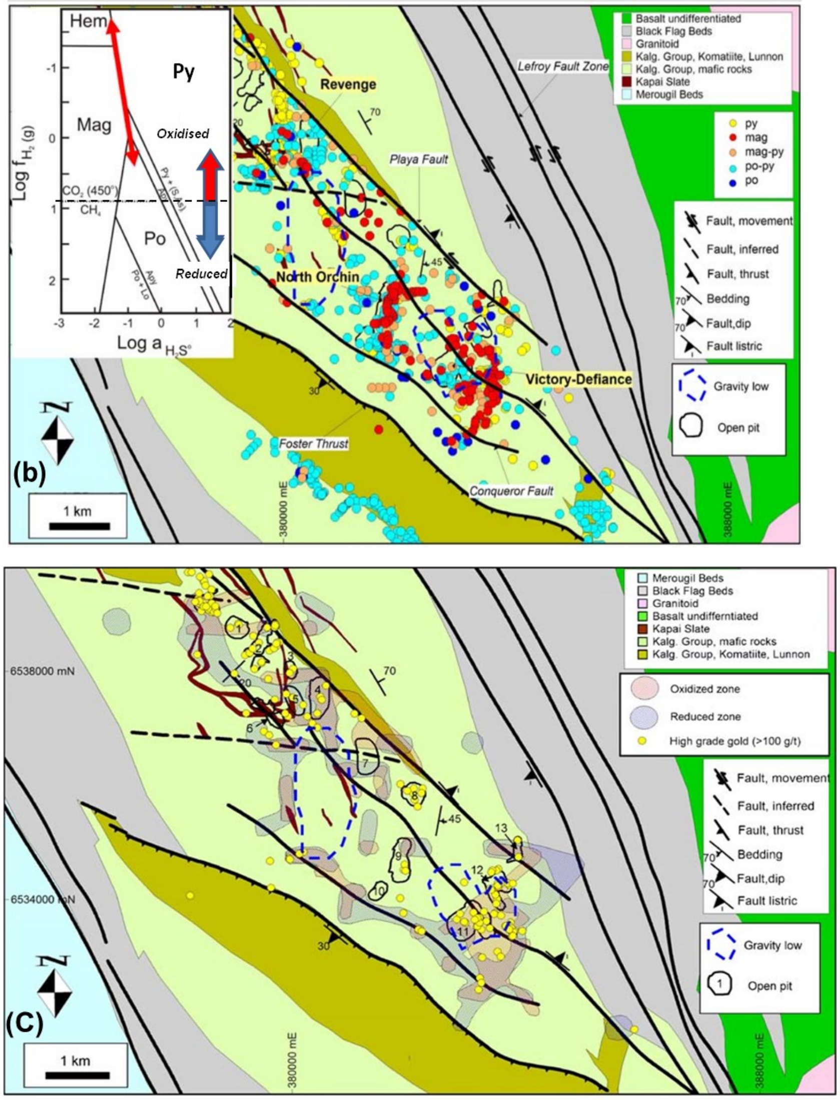

Figure 7.1. Examples of fluid mixing scenarios. (a) A model where oxidised meteoric water form high level sedimentary basins and oxidised $CO_2 - SO_2$ fluids from a crystallising granite mix with reduced $H_2 - CH_4 - N_2$ fluids derived from deep in the crust or mantle and focussed into a fault, to produced isolated lenses (yellow) of gold mineralisation. (b) A map of the St. Ives gold field in the Yilgarn of Western Australia. The mineral assemblages are interpreted as oxidised (magnetite) and reduced (pyrrhotite- pyrite) so that the area is a "sea" of reduced (blue) assemblages punctuated by oxidised (red) fluids. Evidently the reduced and oxidised fluids are synchronous. Gold is deposited at the boundary between the two redox regimes. (c) The St. Ives goldfield with high grade (≥100 g/t) gold deposits superimposed on regions of oxidised and reduced mineral assemblages.

The mineral reactions occurring in Figure 7.1 (b) involve, *inter alia*, reactions of the form:

$$CH_{4(aq)} + SO_{4(aq)}^{2-} + 2H^{+} \rightleftarrows H_{2}CO_{3(aq)} + H_{2}S_{(aq)} + H_{2}O_{(l)} \qquad (7.1)$$

If one considers (as is usually done) the system to be closed (a difficult concept to understand since at least $CH_{4(aq)}, SO_{4(aq)}^{2-}$ and H^{+} are added to the system) then one arrives at the equilibrium phase diagram shown in the insert to Figure 7.1 (b). If however the system is considered open to the influx of $CH_{4(aq)}, SO_{4(aq)}^{2-}$ and H^{+} then the situation and the outcome are quite different. We consider the details of such situations in Chapter 8 but briefly pursue the argument here. We define the extent of the reaction (7.1) as $\xi = \frac{a^0_{\mathrm{CH}_{4(aq)}} - a_{\mathrm{CH}_{4(aq)}}}{a^0_{\mathrm{CH}_{4(aq)}}}$ where $a^0_{\mathrm{CH}_{4(aq)}}$ is the activity of CH_4 at the inlet of the system and $a_{\mathrm{CH}_{4(aq)}}$ is the instantaneous activity of CH_4 as the reaction (7.1) proceeds. When $a_{\mathrm{CH}_{4(aq)}} \to a^0_{\mathrm{CH}_{4(aq)}}$, $\xi \to 0$ and the system is reduced; as the reaction approaches completion, $a_{\mathrm{CH}_{4(aq)}} \to 0$, $\xi \to 1$ and the system becomes more oxidised.

In a situation where the system is closed the rate of a chemical reaction can be considered to be solely a function of the rate constant for the reaction. Since the system is closed the second law of thermodynamics says that the only stable state for the system is chemical equilibrium so that the phase diagram shown in the inset to Figure 7.1 (b) results. In open flow systems (Chapter 8) the rate of a chemical reaction is a function not only of the rate constant for the reaction but also the net inflow of reactants (and heat) to the system. The result in the simplest of cases is that the extent of the reaction is a function of the net flow rate of reactants as shown in Figure 7.2 (a).

The plot of the reaction rate against the extent of the reaction is of the form shown in Figures 7.2 (a, b) whereas the plot of net inflow rate against the extent is a straight line for this simple situation and is shown as a red line in Figures 7.2 (a, b). The intersection of the flow rate with the reaction rate represents a non-equilibrium stationary state. A number of these stationary states are considered in Figure 7.1 (b). Some stationary states are stable, some are unstable, some represent a situation where the supply of reactants is slow but just able to “ignite” the reaction whereas others represent states where the flow is too fast for the reaction and the reaction is “extinguished” (the residence time is too small). Another way of thinking of the system is shown in Figure 7.1 (b) where the various forms of behaviour are represented by the red curve in the centre of the diagram. This curve is shown in more detail in Figure 7.1 (c).

Examination of (7.1) shows that as the extent of the reaction increases the redox state becomes more oxidised so that if the extent is expressed in terms of the redox state at constant activity of H_2S then we obtain Figure 7.2 (d). Magnetite is stable under conditions corresponding to the upper (oxidised) branch of the curve whereas pyrrhotite is stable under conditions corresponding to the lower (reduced) branch.

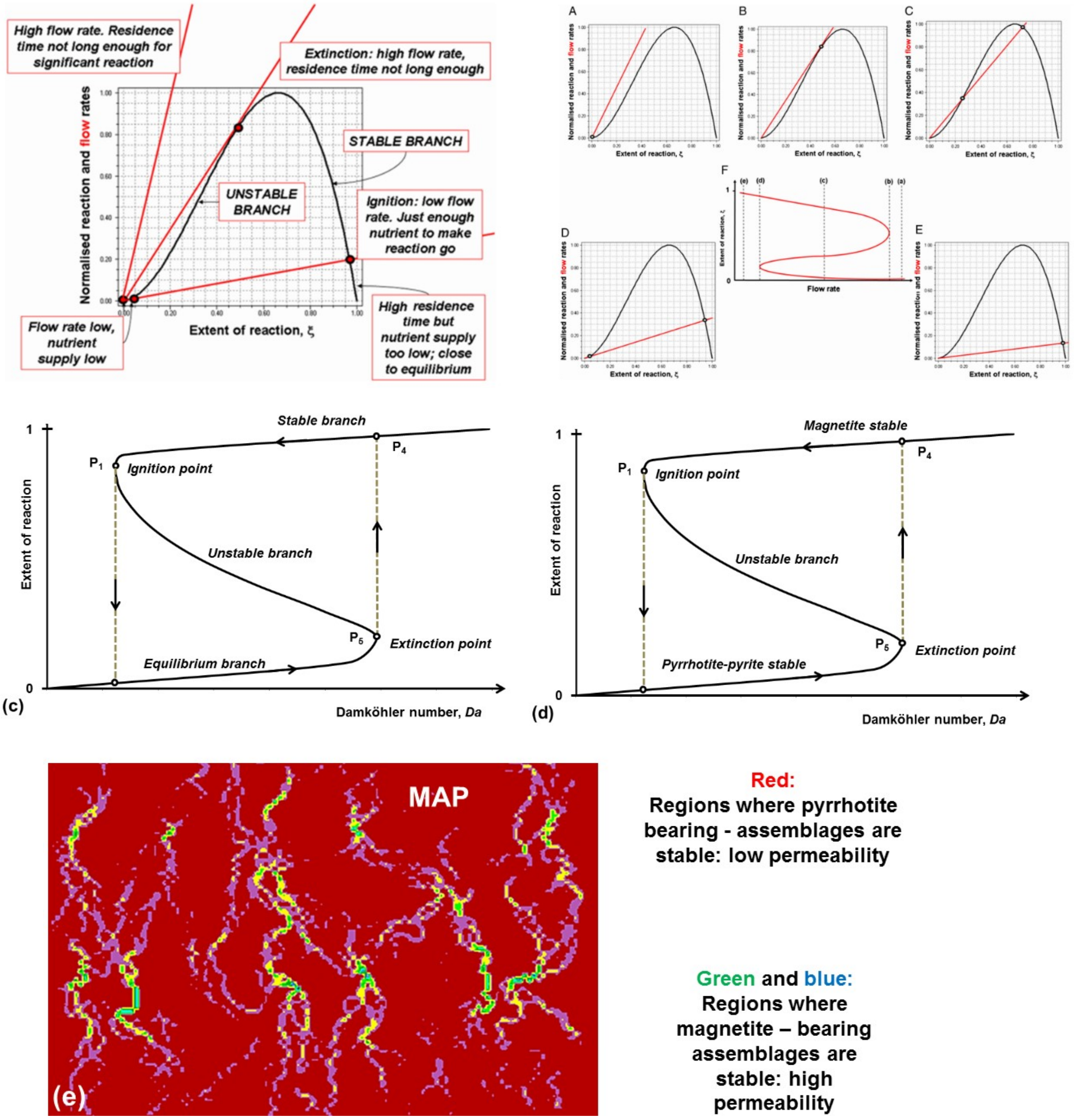

Figure 7.2. The kinetics of simple reactions in an open flow system. (a) Reaction rate and flow rate plotted against the extent of the reaction. The flow rate in this situation is a linear function of the extent of the reaction. (b) Various stationary states that arise in Figure (a) and (centre) the resulting plot of extent of reaction against flow rate. (c) Details of the central diagram of (b). (d) The diagram shown in (c) interpreted in terms of redox state and mineral assemblages. The mineral assemblages here are non-equilibrium stable assemblages. (e) A map showing distribution of redox states expressed as mineral assemblages. The distribution is a direct result of (d) where the assemblage is controlled by the flow rate (in turn controlled by the permeability) and not by fluid mixing.

As the flow rate increases the system first follows the lower branch of Figure 7.2 (c, d) where (reduced) pyrrhotite-bearing assemblages are stable. At the point A the system switches discontinuously to the upper branch where (oxidised) magnetite is stable. Both of these stability conditions represent non-equilibrium stable states (Ross, 2008). The system is held away from equilibrium by the influx of $CH_{4(aq)}, SO^{2-}_{4(aq)}$ and H^+ but stable non-equlibrium states can exist (Ross, 2008; Gray and Scott, 2010). The situation is equivalent to a system with a heterogeneous permeability distribution so that regions of different flow rates occur togther spatially as in Figure 7.2 (e). Thus what appears to be a system involving the influx of fluids with different redox states is actually the result of a single fluid reacting with the country rock but with different flow rates corresponding to regions of different permeability. Gold is deposited not as a result of a change in oxidation arising from fluid mixing, but as a result of the coupled reactions of the form:

$$H_2CO_{3(aq)} + H_2S_{(aq)} + H_2O_{(l)} \rightarrow CH_{4(aq)} + SO^{2-}_{4(aq)} + 2H^+$$

$$AuHS(H_2S)^0_{3(aq)} + 0.5H_2 \rightarrow Au_{(solid)} + 4H_2S_{(aq)}$$

with different flow rates in different regions. We explore this system in more detail in Chapter 8. One should note that the reaction kinetics shown in Figure 7.2 are for the simplest system possible where the flow rate is a linear function of the extent of reaction. For more complex situations this relation is nonlinear and more complicated forms of Figure 7.2 arise allowing assemblages with haematite, magnetite and pyrrhotite to form from the same fluid. We consider these situations in Chapter 8. The exploration significance of contrasted redox states remains but the influx of multiple fluids with different compositions is not required. In principle there should be a correlation between the distribution of gold and the permeability at the time of fluid influx but this may be difficult to establish and measure.

2. Chaotic and turbulent flows.

Although fluid mixing must be involved in the dissolution and reaction processes within pore spaces and at fluid-solid boundaries and is widely proposed as an important ingredient in the formation of hydrothermal systems, it remains very poorly understood (Ord et al., 2012). We describe *fluid mixing* as the dispersion of constituent species through the actions of fluid advection and/or molecular diffusion toward a spatially homogeneous distribution.

Mixing of two fluids can occur in three ways:

(i) Two laminar flowing fluid streams may meet and mix by molecular diffusion across the interface between the fluids; this is the process commonly inferred in the geological literature.

(ii) Differences in the chemical or physical properties of the two fluid streams (for instance chemical potential, density, surface tension, temperature) generate flow instabilities at the interfaces between the fluids which enhance fluid mixing (De Wit, 2001, 2008). Examples of such instabilities are given in Figures 7.3 and 7.4.

(iii) Two fluid streams may meet in an open three dimensional network, either at the grain-scale, where the network comprises a series of interconnected pores between grains, or at larger scales where the network comprises a series of interconnected open fractures (Figure 7.5). The inherent three dimensional geometric complexity of these networks (Ord et al., 2012; Lester et al., 2012, 2016) results in a flow phenomenon known as *chaotic advection*, that is, fluid particle trajectories form a chaotic tangle, leading to efficient mixing (Figure 7.6).

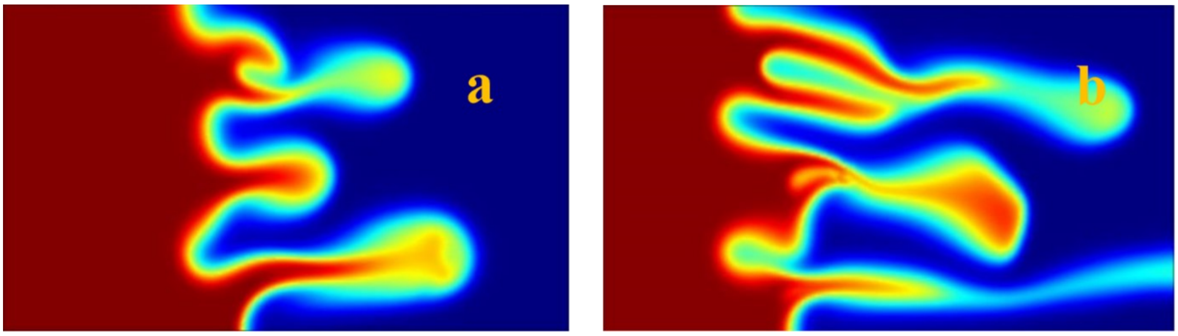

Figure 7.3. Concentration distributions for a moving front between two reacting fluids (A) Lewis number = 10. (b) Lewis number = 1 (From Liu, 2014). The Lewis number is a measure of the importace of heat transport by diffusion to mass transport. Mass transport becomes more important as the Lewis number decreases.

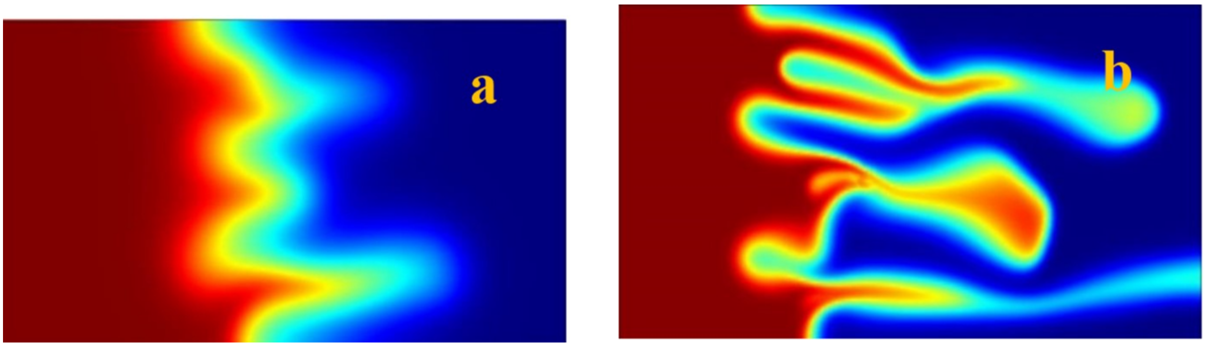

Figure 7.4. Temperature distributions for a moving front between two reacting fluids (A) Lewis number = 10. (b) Lewis number = 1 (From Liu, 2014).

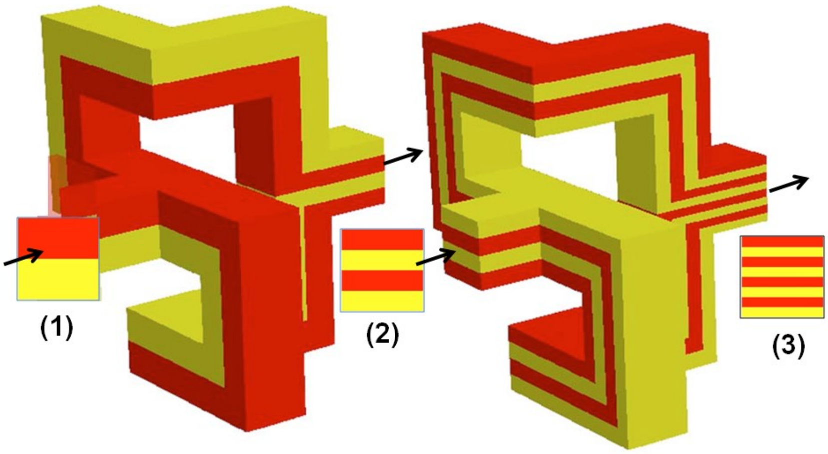

Figure 7.5. Chaotic advection in a three dimensional network with branching and merging pore or fracture space. After Carrière (2007). The fluid is stretched and compressed as it traverses each set of pores from (1) to (2) to (3). The ultimate result is a Baker’s transform where two initially adjacent fluids (red and yellow) are brought together as finer and finer striae.

The first mixing mechanism above involves diffusion alone, and is not efficient since the molecular diffusivity, *D*, for relevant aqueous species is typically of magnitude 10^{-10} m^2 s^{-1}. Thus the time scale for mixing over a distance of 100 m is 3 million years. The issue is discussed by Appold and Garven (2000).

The latter two mechanisms involve the interplay of advection and diffusion, the relative timescales of which are characterised by the molecular Peclet number, $\mathrm{Pe}^{molecular}$ (see Chapter 3). For $\mathrm{Pe}^{molecular} \leq 1$ chemical reactions are dominated by reaction–diffusion (RD) processes (see Chapter 8). Chaotic mixing involving laminar flow occurs in the range $1 < \mathrm{Pe}^{molecular} < 10^7$ but enhanced chemical reaction rates due to chaotic flow occur only for $10^2 < \mathrm{Pe}^{molecular} < 10^7$ (see Chapter 3; Tel et al., 2000, 2005; Ord et al., 2012). Turbulent mixing begins at $\mathrm{Pe}^{molecular} = 10^7$ (Villermaux, 2012), corresponding to a Reynolds number of $\approx 10^3$. Turbulent flow results in enhanced chemical reaction rates (Villermaux, 2012) but turbulent flow is unlikely in crustal systems except for large hydrothermal breccia systems. Below the threshold $\mathrm{Pe}^{molecular} = 1$, the effect of mixing arising from fluid advection upon chemical reaction rates is negligible and diffusion dominates, whereas above the threshold $\mathrm{Pe}^{molecular} = 10^2$ advection can enhance mixing rates by several orders of magnitude.

Fluid advection not only has a profound effect upon mixing rates, but can also alter the stability and speciation of non-equilibrium chemical reactions (Tel et al., 2005) such as those encountered in hydrothermal systems. Hence the threshold Peclet numbers not only represent approximate thresholds in terms of mixing rate, but also the qualitative properties of mineral reaction and deposition are expected to differ across these thresholds. Although fluid advection is important below $\mathrm{Pe}^{molecular} = 10^2$ for transporting, reacting mineralizing systems, the argument above suggests that these latter systems may be validly treated as RD systems. Above this transition the reactions are better treated as advection–diffusion–reaction (ADR) systems (Chapter 8). Although the literature on RD systems is immense, ADR systems have enjoyed much less attention. A review of some aspects of ADR systems is Neufeld and Hernandez-Garcia (2009).

In order to understand the mechanisms by which fluid advection accelerates fluid mixing in hydrothermal systems, we provide a brief overview of the phenomenon of chaotic advection, involving terms and concepts which may be unfamiliar to the geoscientist. The reader is directed to several review articles (Metcalfe, 2010; Ottino, 1989; Tel et al., 2000, 2005; Wiggins and Ottino, 2004) for further reading. The ability of turbulent flows rapidly to mix and disperse constituents is a widely recognized phenomenon (Villermaux, 2012). Turbulent flows possess a wide spectrum of eddy length-scales, which act to distort concentration fields into complex spatial distributions with very fine striations and large interfacial area between constituents of the flow thus accelerating reaction rates. In conjunction with molecular diffusion, such fluid advection leads to rapid dispersion, which is commonly termed mixing. Dispersion occurs even if the molecular diffusivity is vanishingly small. Conversely, slow, laminar flows are smooth and regular, and do not possess small length scales for the organization of fluid elements into fine striations.

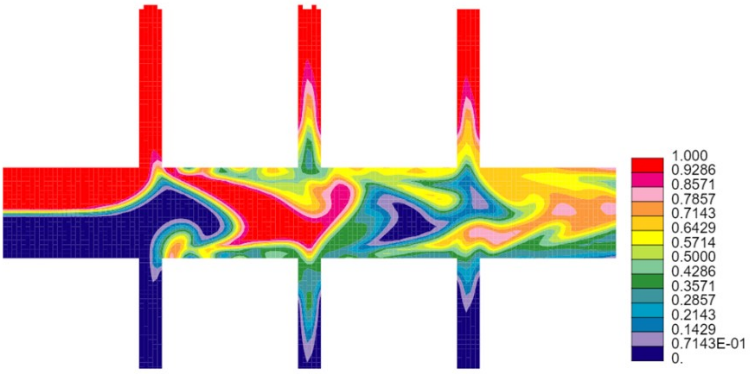

Figure 7.6. An example of chaotic mixing in which the fluid flow is laminar. The flow in the horizontal tube is stationary and fluid mixing is produced by periodic influx of fluid from the side channels. The concentration shown is that of a non-reactive scalar (red: full concentration; dark blue: zero concentration). From Tel et al. (2005). The flow may appear turbulent but at each instant the flow is laminar.

As such, slow molecular diffusion usually does little to accelerate dispersion in steady laminar flows. The transition from laminar to turbulent flow typically occurs at Reynolds number Re ~ 10^3. We can express Re as:

$$\mathrm{Re} = \frac{\mathrm{Pe}}{\mathrm{Sc}} = \frac{\textit{viscous diffusion}}{\textit{molecular diffusion}}$$

where $\mathrm{Sc} = \mu^{fluid}/\rho^{fluid}D$ is the *Schmidt number* quantifying the ratio of viscous diffusion to molecular diffusion; ρ^{fluid} and μ^{fluid} are the fluid density and viscosity respectively. The Schmidt number is a material property, typically 10^3 to 10^4 for aqueous systems (as $\rho^{fluid} \sim 10^3$ kg m^{-3}, $\mu^{fluid} \sim 10^{-3}$ to 10^{-4} Pa s, $D \sim 10^{-10}$ m^2 s^{-1}), and so Re = 10^{-4} Pe to 10^{-3} Pe.

Whilst this may be true for a wide range of laminar flows, there exist important exceptions that would seem to be the common situation in hydrothermal systems and that arise when the laminar flows are unsteady. Then the opportunity exists for the streamlines (which never intersect at any instant of the flow) to cross from one instant to the next. Although the Eulerian description of the flow is always laminar, the particle track for any material particle can become chaotic (Metcalfe, 2010; Ottino, 1990). This arises because the kinematic advection equation,

$$\frac{\mathrm{d}\boldsymbol{x}}{\mathrm{d}t} = \boldsymbol{v}\left(\boldsymbol{x}, t\right)$$

describing the evolution with time t of the position $\boldsymbol{x}$ of a passive fluid tracer particle under the action of the fluid velocity field $\boldsymbol{v}$, is a nonlinear dynamical system capable of exhibiting chaotic dynamics. As such, although the velocity field $\boldsymbol{v}(\boldsymbol{x}, t)$ itself is smooth, the fluid particle trajectories may be chaotic, leading to rapid dispersion and mixing. This phenomenon is termed *chaotic advection* (Aref, 1984; Ottino, 1990), and has been well studied over the past quarter century in the fields of fluid mechanics and dynamical systems. One familiar example of chaotic advection is expressed as the *Baker's transform*, examples of which are the kneading of bread dough or the manufacture of salt-water taffy. Kneading may be considered as a laminar flow comprising of iterated stretching and folding motions. Although the flow field associated with these motions is smooth and regular, if one were to track the evolution of a dyed element of dough or taffy, it would soon be stretched to form a highly striated distribution and eventually be mixed throughout the dough or taffy form. This is chaotic advection in action. The actions of stretching and folding are in fact the fundamental mechanisms of chaotic dynamics in general: stretching acts to separate particles at an exponential rate, and folding acts to reorganize the flow to distribute these highly striated interwoven structures throughout the domain. Figure 7.4 provides an example of the Baker's transform for flow in a three dimensional pore or fracture network.

The rate of exponential stretching is quantified by the *Lyapunov exponent*, λ, which is taken as a measure of the strength of the chaotic dynamics. In the case of chaotic advection, the Lyapunov exponent is defined as the long time limit of the exponential growth rate of the length of a material line $\delta\boldsymbol{x}$ between two particles initially separated by distance $\delta\boldsymbol{X}$

$$\lambda = \lim_{t\to\infty} \frac{1}{t} \ln \frac{|\delta\boldsymbol{x}|}{|\delta\boldsymbol{X}|}$$

Whilst the flow domain may be finite-sized, $|\delta\boldsymbol{x}|$ can grow without bound due to the interwoven nature of the striations and hence of the initial material line. Although chaotic particle paths appear to be irregular and random, their underlying structures are highly organized and are often self-similar and multifractal (Muzzio et al., 1992). This organizing structure is termed the *chaotic template*, and active processes within the fluid such as diffusion and reaction play out on this template.

Although many laminar flows are engineered to exhibit chaotic advection to promote mixing and dispersion in a wide variety of applications, chaotic advection can occur in natural flows also. Systems subject to transient forcing or flow reorientation can exhibit chaotic advection, such as the evolution of plankton communities in oceanic currents (Hernandez-Garcia and Lopez, 2004; Karolyi et al., 1999) or the spreading of the gulf oil spill (Mezić et al., 2010; Thiffeault, 2010). Flows in porous media subject to transient forcing have been shown (Jones and Aref, 1988; Lester et al., 2009, 2010, 2016; Metcalfe et al., 2010a, 2010b; Trefry et al., 2012; Zhang et al., 2009) to exhibit chaotic advection again due to the stretching and folding motions of the transient flow field. Recent studies (Carrière, 2007; Lester et al., 2012) have also established the propensity for chaotic advection to occur in porous media under steady flow, via the natural tortuosity of the pore-space (figure 3.14). Mixing due to chaotic flow has also been described in nano-porous networks (Ottino and Wiggins, 2004 and references therein) and rapid developments are happening in this area which have direct application to fluid transport and mineral reactions in hydrothermal systems.

7. 3. An example of fluid mixing relevant to unconformity uranium deposits.

A common model for unconformity related uranium deposits is illustrated in Figure 7.7. Fluid flow is envisaged in an aquifer that overlies a basement where a fault discharges fluid from the basement into the aquifer fluid. The basement fluid is reduced (due to the presence of carbon) and the basinal fluids are oxidised. Uranium is deposited, arising from mixing of the two fluids. Most mineralisation occurs in the fault or at the unconformity but there is mineralisation in the aquifer above the intersection of the fault with the unconformity (Wallis et al., 1983).

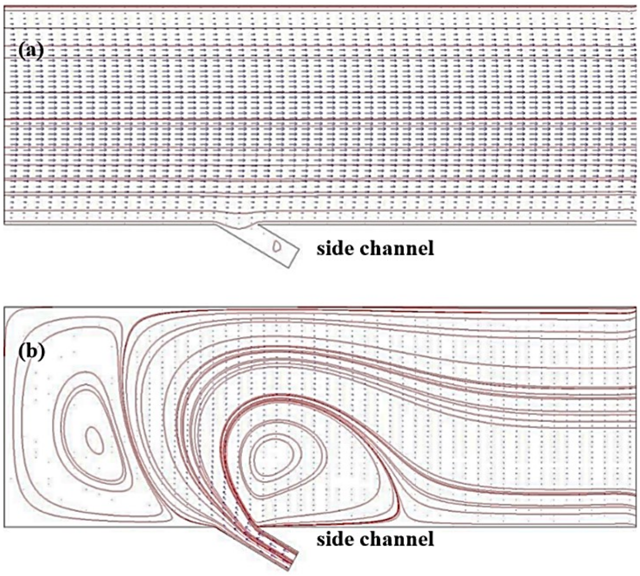

Figure 7.7. Geometry of the model. (a) Initial set up with fluid flowing horizontally to the right and fluid of a different composition injected in the basement fault which is labelled as a side channel. (b) the resulting streamline configuration.

Figure 7.7 shows the chaotic mixing that occurs from the injection of fluid from the basement fault (labelled “side channel” in Figure 7.7) into the aquifer fluid. Most fluid ultimately leaves the system, as shown by Figures 7.8 and 7.9 but one position, above but downstream from the fault remains as a position of strong fluid mixing.

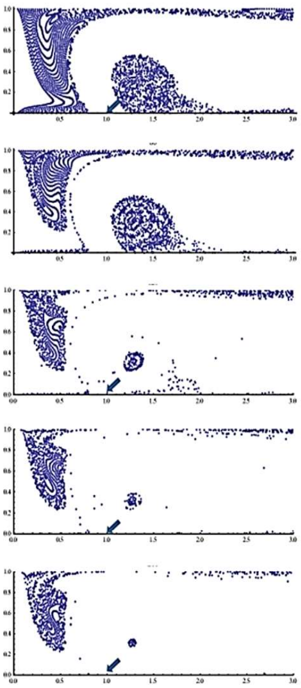

Figure 7.8. Fluid particle tracks during the evolution of the flow. The side channel is marked with an arrow. Time progresses from top to bottom. As time proceeds most of the initial fluid is swept from the system but a concentration of particles remains just above and downstream from the side cannel.

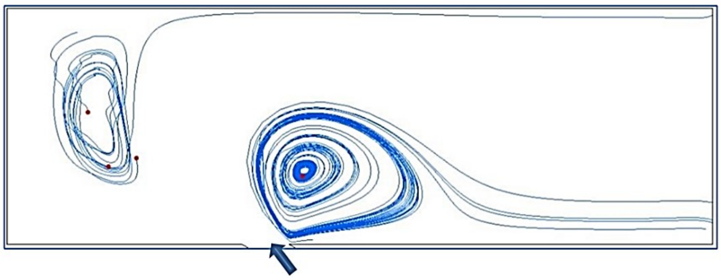

Figure 7.9. Another view of the evolution of the system. The system begins with many equally spaced particles. At the stage represented in the figure, only four particles remain but the subsystem above and downstream from the side channel remains a stable position of strong fluid mixing.

7. 4. Summary.

The mixing of two fluids with contrasting redox states is a common model for producing mineralisation. The model is based on observations that mineralisation is commonly localised at or near the interface between rock units with mineral assemblages corresponding to different redox states. However the mixing of two fluids across a planar interface is very slow and represents a very inefficient mixing process. Efficient mixing occurs at the interface between two reacting fluids arising from instabilities in the reaction front. However the most efficient mixing process is that of so called *chaotic mixing* where the flow is laminar but unsteady so that stream lines cross from one instant to the next. This pattern of mixing is quite distinct from turbulent mixing where a cascade of eddies also leads to efficient mixing. The most common means of generating non-turbulent chaotic fluid mixing is by the flow of two fluids through a three dimensional network of pores (including fractures) so that stream lines are forced by the geometry of the network to cross and distort each other resulting in chaotic mixing.

It is important to note that all alteration systems that consist of oxidised mineral assemblages embedded in reduced assemblages (or *vice versa*) may not be evidence of the interplay of two fluids. Some patterns of this type can result from a single reactive fluid invading rock with heterogeneous permeability; then the oxidised and reduced mineral assemblages are the result of contrasted fluid velocities arising from different permeabilities.

Recommend reading.